RSC Advances

ROYAL SOCIETY OF CHEMISTRY

www.rsc.org/advances

One-pot catalytic conversion of methanol to C6–C21 hydrocarbons over bi-functional MFe_2O_4 (M = Ni, Zn, Mn, Co) catalysts

Huilong Lai,[a,b] Zailei Zhang,[b] Fangna Gu,[b,*] Zhengming Yi,[a,*] Ziyi Zhong,[c] and Fabing Su[b,*]

[a] *School of Chemical Engineering, Xiangtan University, Xiangtan 411105, Hunan, China*

[b] *State Key Laboratory of Multiphase Complex Systems, Institute of Process Engineering, Chinese Academy of Sciences, Beijing 100190, China*

[c] *Institute of Chemical Engineering and Sciences, A*star, 1 Pesek Road, Jurong Island, Singapore 627833, Singapore*

*Corresponding author: fngu@ipe.ac.cn (F. Gu); YIZM@xtu.edu.cn (Z. Yi); fbsu@ipe.ac.cn (F. Su), Tel.: +86-10-82544850; Fax: +86-10-82544851

Abstract

We report a novel catalytic conversion of methanol to C6–C21 hydrocarbons over the bi-functional MFe_2O_4 (M = Ni, Zn, Mn, Co) catalysts prepared by a solvothermal method. The process consists of two steps: (i) the catalytic reforming of methanol to H_2 and CO, and (ii) the subsequent conversion of the syngas to hydrocarbons via Fischer-Tropsch synthesis (FTS). For the comparison purpose, two other series of catalysts including MO (M = Ni, Zn, Mn, Co, Fe), and $M_{0.5}Co_{0.5}Fe_2O_4$ (M = Ni, Zn, Mn) catalysts were also prepared and tested. All the catalysts were characterized by X-ray diffraction, nitrogen adsorption, transmission electron microscopy, scanning electron microscopy, and H_2-temperature programmed reduction. Among these catalysts, $ZnFe_2O_4$ exhibited the highest activity with a high methanol conversion of 26% and a high selectivity to C6–C21 hydrocarbons above 94% at 300 ^oC. Moreover, this $ZnFe_2O_4$ catalyst was still stable and reusable after 4 runs under the reaction conditions. This work demonstrates a possibility to directly convert methanol to liquid fuels.

Key words: Catalytic conversion; Methanol; C6–C21 hydrocarbons; Fe-based bi-functional catalysts

1. Introduction

With the increasing depletion of petroleum resources and growing concerns over the global climate change, production of fuels from renewable and low-cost resources such as bio-methanol has attracted tremendous attentions because of the high sustainability and environmental benignity of this approach.[1] Although methanol itself is a potential motor fuel or can be blended with gasoline, large investment would be required to overcome the technical problems connected with the direct use of methanol as a fuel. Therefore, recently some researchers have paid much attention to catalytic reforming of methanol to syngas, which can be further converted to various fuels and fuel additives through FTS.[2] The reported catalysts for methanol reforming are mainly copper-based and group VIII metal-based catalysts.[3-6] However, the copper-based catalysts suffer from some problems such as pyrophoric phenomenon and easy deactivation caused by thermal sintering.[7, 8] Compared with these Cu-based catalysts, it seems group VIII catalysts have better resistance to sintering and long-term stability.[9, 10]

In the past decades, the catalysts based on group VIII metals such as Fe, Co, Ru, Rh and Ni were extensively investigated for FTS.[11-15] In order to improve the catalytic performance, promoted catalysts, e.g., K promoted Fe catalyst,[16] and bimetallic catalysts with generated synergistic geometric and electronic effects, e.g., cobalt ruthenium catalysts[17] were tested. In general, the catalytic activity of VIII metals for FTS is in the order of Ru > Fe > Ni > Co > Ph > Pd > Pt.[18] Although Ru catalysts show the highest yield for high-carbon hydrocarbons and low selectivity for methane, the high price and limited resource of Ru restricts their application. Hence, most reported catalysts are still Fe-, Ni- and Co-based catalysts. Even though oil companies around the world have developed their patented FTS technology and processes, which usually start from coal gasification, desulfurization and decarbonization to syngas, followed with conversion of the syngas to

hydrocarbons.[19, 20] This process is very mature but quite complicated. We had wondered for a long time whether the methanol reforming reaction and the FTS of syngas could be integrated into a one-pot process to produce hydrocarbons using bi-functional catalysts.

Herein, we report a novel one-pot catalytic conversion of methanol to C6–C21 hydrocarbons over Fe-based spinel MFe_2O_4 (M = Ni, Zn, Mn, Co) catalysts synthesized by a simple solvothermal method. It is found that in the conversion of methanol, the bi-functional Fe-based spinel catalysts firstly catalyze methanol reforming to generate H_2 and CO, and then convert these gas products to C6–C21 hydrocarbons. Among these catalysts, $ZnFe_2O_4$ shows the best catalytic properties and good stability. The major liquid products containing C6–C21 hydrocarbons produced by this method can be used as diesel and jet fuel.

2. Experimental section

2.1. Catalyst preparation

All the chemicals of analytical grade were purchased from Sinopharm Chemical Reagent Co. Ltd., China, and used without further treatment. All the catalysts were prepared by a solvothermal method, and the used reactant, mineralizer and solvent and their amounts are listed in Table S1. In a typical synthesis, $Zn(CH_3COO)_2{\bullet}4H_2O$ (1.0 mmol), $FeCl_3{\bullet}6H_2O$ (2.0 mmol), and $CH_3COONa{\bullet}3H_2O$ (18 mmol) were dissolved in a solution of $HOCH_2CH_2OH$ (40.0 mL) and deionized water (40.0 mL) to form a homogeneous slurry by stirring, which was subsequently sealed in a stainless-steel autoclave and heated at 200 ^oC for 48 h to obtain the desired products.[21] The resulting precipitate was collected by centrifugation, washed with distilled water and absolute ethanol, and finally dried in vacuum at 80 °C for 24 h. The synthesized samples was denoted as MFe_2O_4 (M = Ni, Zn, Mn, Co). Likewise, single metal oxide of MO (M = Ni, Zn, Mn, Co, Fe)

catalysts and ternary metal oxides of $M_{0.5}Co_{0.5}Fe_2O_4$ (M = Ni, Zn, Mn) catalysts were prepared by the same method but with addition of only one metal salt or three metal salts.

2.2. Characterization

The X-ray powder diffraction patterns of the samples were obtained with a PRO (PANalytical) diffractometer operated at 40 kV and 40 mA by using Cu Kα radiation (λ = 1.5418Å). The crystal size was calculated using the Debye-Scherrer equation. The microscopic feature of the samples was characterized by field-emission scanning electron microscopy (SEM) with an energy dispersive X-ray spectrometer (EDX) (JSM-7001F, JEOL, Tokyo, Japan) and transmission electron microscopy (TEM) (JEM-2010F, JEOL, Tokyo, Japan). Adsorption-desorption isotherms were measured using N_2 at −196 ^oC with NOVA 3200e (Quantachrome, USA) nitrogen adsorption apparatus. Before measurement, the sample was degassed at 200 ^oC for 5 h under vacuum. The specific surface area was determined according to the Brunauer-Emmett-Teller (BET) method in the relative pressure range of 0.05–0.2. Temperature-programmed reduction with H_2 (H_2-TPR) was carried out on an automated chemisorption analyzer (chem-BET pulsar TPR/TPD, Quantachrome). Prior to the measurement, 0.1 g of catalyst placed in a quartz U-tube was pretreated in an Ar stream at 300 ^oC for 1 h. Then, the sample was cooled to room temperature, followed by heating to 1000 ^oC at 10 ^oC min^{-1} under a binary gas (10.0 vol. % H_2/Ar) with a gas flow of 30 mL min^{-1}. The surface chemical composition of the samples was determined by X-ray photoelectron spectroscopy (XPS) on a VG ESCALAB 250 spectrometer (Thermo Electron, U.K.), using a nonmonochromatized Al Kα X-raysource (1486 eV). The binding energies were calibrated using C1s peak of contaminant carbon (BE = 284.6 eV) as an internal standard.

2.3. Catalyst evaluation

In a typical run, 0.1–0.9 g catalyst and 30 mL methanol (Tianjin Xihua Special Type Reagent Factory, China) were put into a 100 mL stainless-steel autoclave reactor (Parr Instrument Company). After purged the reactor with nitrogen, the reaction was carried out at a given temperature between 240–340 ^{o}C for a certain time (10–240 min) under a continuous stirring at 400 rpm. After the reaction, the reactor was cooled down to room temperature. The gas products were collected by a gas bag and analyzed by a Micro GC (3000A; Agilent Technologies) equipped with a thermal conductivity detector (TCD). The liquid products were separated from the catalyst by filtration and analyzed by gas chromatography/mass spectrometry (GCMS-QP2010 Ultra, Shimadzu) with a 30 m×0.25 mm, and 0.25 μm film thickness RX-5ms column. The compound was determined by the computer software from the characterized GC/MS graphs. The residue methanol in the liquid products were analyzed by GC (9790; Zhejiang Fuli Analytical Instrument CO., LTD) equipped with a hydrogen flame ionization detector (FID). The liquid products over different catalysts were classified into five groups, namely hydrocarbons, alcohols, methyl esters, ketones, and others. The GC peak area and peak area % of each product were employed to compare the relative content among the detected products.[22, 23] each group liquid products were analyzed at least three times and the average values of peak area and peak area % were calculated for discussion.[24] Methanol conversion was calculated using the following formulas:

$$\text{methanol conversion} = \frac{\text{Mass}_{\text{methanol}} - \text{Mass}_{\text{residue}}}{\text{Mass}_{\text{methanol}}} \times 100\% \qquad (1)$$

Where $\text{Mass}_{methanol}$ is the mass of methanol used, $\text{Mass}_{residue}$ is the mass of residual methanol after reaction.

The stability of catalytic activity was tested at 300 ^{o}C and 120 min for 4 runs. The catalyst after reaction was washed with deionized water and ethanol several times for next run.

3. Results and discussion

3.1. Characterization

Fig. 1a-1b show the XRD patterns of the fresh MO (M = Zn, Co, Fe, Ni, Mn) and MFe_2O_4 (M = Ni, Zn, Mn, Co) catalysts. The typical diffraction peaks of MO and MFe_2O_4 match well with their corresponding PDF files. Fig. 1c shows the XRD patterns of $M_{0.5}Co_{0.5}Fe_2O_4$ (M = Ni, Zn, Mn) catalysts before the reaction. The typical diffraction peaks of $Ni_{0.5}Co_{0.5}Fe_2O_4$,[25] $Zn_{0.5}Co_{0.5}Fe_2O_4$[26] and $Mn_{0.5}Co_{0.5}Fe_2O_4$[27] appear in the XRD patterns of $Ni_{0.5}Co_{0.5}Fe_2O_4$, $Zn_{0.5}Co_{0.5}Fe_2O_4$ and $Mn_{0.5}Co_{0.5}Fe_2O_4$ catalysts, respectively, indicating the successful synthesis of MFe_2O_4 (M = Mn, Ni, Zn, Co) and $M_{0.5}Co_{0.5}Fe_2O_4$ (M = Mn, Ni, Zn) with the spinel structure by the solvothermal method. The crystal size was calculated by Scherrer equation and summarized in Table 1. The particle sizes of the MO catalysts are varied in a wide range. Among them, NiO and Mn_3O_4 have a similar size of ca. 42 nm, while Fe_3O_4 and ZnO have a size distribution of 93–102 nm, and the size of Co_3O_4 is about 82.8 nm. Comparing to the MO (M = Zn, Co, Fe, Ni, Mn) catalysts, both MFe_2O_4 (M = Ni, Zn, Mn, Co) and $M_{0.5}Co_{0.5}Fe_2O_4$ (M = Ni, Zn, Mn) have much smaller particle sizes (10–30 nm). The H_2-TPR curves of the MFe_2O_4 (M = Zn, Mn, Co) catalysts (Fig. 1d) show that the $MnFe_2O_4$ (M = Zn, Mn, Co) catalysts were not reduced below 340 ^oC under the H_2-TPR test condition. The XPS spectra of $ZnFe_2O_4$ catalyst reduced at 340 ^oC with H_2 are given in Fig. S1. The signals at 1044.7 and 1021.4 eV can be attributed to Zn $2p_{1/2}$ and Zn $2p_{3/2}$ of Zn^{2+}.[28] Additionally, the signals at around 711.6 and 725.5 eV are from Fe^{3+} at octahedral sites.[29] These results confirm that $ZnFe_2O_4$ cannot be reduced at 340 ^oC under H_2-TPR condition. Fig. S2a shows the XRD patterns of the MFe_2O_4 and $Mn_{0.5}Co_{0.5}Fe_2O_4$ catalysts after reaction. For all the used catalysts, some new diffraction peaks appear at 26.6 and 32.5^o, attributing to carbon (03-065-6212) and $FeCO_3$

(00-003-46) respectively, and a group of diffraction peaks at 36.9°, 32.9°, corresponding to FeC_2 (03-065-1456). The Fe^{3+} can be reduced to Fe^{2+} by the CO produced by methanol reforming.[30] Carbon is formed through the disproportionation reaction of CO. It is possible that CO_2 formed by the water-gas shift reaction plays a key role in the formation of $FeCO_3$. These results indicate a small amount of Fe-based spinel catalysts can be reduced during methanol conversion reaction. Moreover, with the increase of reaction temperature from 220 to 340 °C, the peak intensity of FeC_2 increases and that of the carbon decreases, indicating that the reduction of Fe^{3+} is promoted at high temperature under the reaction conditions (Fig. S2b). The peak intensity of carbon increases with the reaction time from 10 to 60 min, and then decreases with prolonging reaction time. With the increase of reaction time from 10 to 240 min, the peak intensity of FeC_2 shows almost no changes (Fig. S2c). Additionally, when the catalyst amount is changed from 0.1 to 0.9 g, there is a gradual increase in the intensity peak of FeC_2. These results suggest that the reaction conditions and the catalyst amount greatly affect the state of the components of the catalysts.

Table 1 compiles the surface area of all the catalysts. The surface areas of the MO catalysts are 0.1-5.7 $m^2\ g^{-1}$, except that of Mn_3O_4 is 45.2 $m^2\ g^{-1}$. Compared with the MO catalysts, the MFe_2O_4 and $M_{0.5}Co_{0.5}Fe_2O_4$ catalysts have larger surface areas, varying from 21.1 to 76.5 $m^2\ g^{-1}$.

Fig. S3 and Fig. 2a display the SEM images of the MO catalysts. As we can see, the MO catalysts show different morphologies, such as sphere-like Fe_3O_4 and M_3O_4, flakiness Co_3O_4 and NiO, rod-shaped ZnO. Fig. 2b-2e display the SEM images of the MFe_2O_4 catalysts. All the MFe_2O_4 catalysts exhibit spherical morphology, and the sizes of them are smaller than that of Fe_3O_4, implying adding second metal salt favors forming smaller particles, which is consistent with the above XRD results. The SEM images of $M_{0.5}Co_{0.5}Fe_2O_4$ show that these samples consist of nanoparticles with a size of 20–30 nm (Fig. 2f-2h), similar to that of the MFe_2O_4 catalysts.

Fig. 3a shows a representative transmission electron microscopy (TEM) image of the $ZnFe_2O_4$ catalyst. It reveals that the nanoparticles sizes of this catalyst are about 30 nm. The HRTEM image of these nanoparticles (Fig. 3b) shows that the lattice fringe spacing is about 0.4847 nm, corresponding to the interplanar distance of (110) planes in $ZnFe_2O_4$. The corresponding elemental mappings for the MFe_2O_4 (M = Zn, Mn, Co) catalysts are displayed in Fig. 3c and Fig. S4-S5. As can be seen, all the elements are evenly distributed within the whole samples. The molar ratios of each element in the final samples are approximately equal to the initial ratios of the metal precursors added in the preparation process (Table S1). The SEM-EDX spectrum of $ZnFe_2O_4$ nanoparticles is given in Fig. 3d, which demonstrates the presence of Zn, Fe, and O elements with an approximate atomic ratio of 1: 2: 4.

3.2. Catalytic conversion of methanol over the MO, MFe_2O_4 and $M_{0.5}Co_{0.5}Fe_2O_4$ catalysts

The catalytic conversion results of methanol over all the catalysts are summarized in Table 2. The blank test (without any catalyst) gives about 8.9% conversion of methanol with a little amount of gas product. After added with the MO (M = Zn, Co, Fe, Ni, Mn) catalysts, the conversion of methanol is increased, which reaches 35.9% over the Co_3O_4 catalyst, implying that the methanol reforming reaction is catalyzed. Meanwhile, MFe_2O_4 and $M_{0.5}Co_{0.5}Fe_2O_4$ exhibit higher conversion of methanol (above 22%) compared with most of the MO catalysts except for the Co_3O_4 and NiO catalysts. The yields of gas products over NiO and Co_3O_4 are similar and highest among all the MO catalysts, and that over Fe_3O_4 is second highest. Among all the MFe_2O_4 catalysts, $NiFe_2O_4$, $ZnFe_2O_4$ and $MnFe_2O_4$ catalysts exhibit higher yield of gas products, whereas the $CoFe_2O_4$ catalyst yields less gas product than the Fe_3O_4 catalyst. It may be because the addition of the second metal element promotes methanol reforming reaction. Additionally, the larger specific surface areas of the formed

$NiFe_2O_4$, $ZnFe_2O_4$ and $MnFe_2O_4$ catalysts may enable them to expose more active sites for methanol reforming reaction. However, the addition of Co element is in favor of methanation reaction, which is a gas volume diminishing reaction. Compared to the MFe_2O_4 catalysts, the yields of the gas products over the $M_{0.5}Co_{0.5}Fe_2O_4$ catalysts are lower, probably due to the fact that the Co element is in favor of methanation reaction.

Fig. 4a shows the distribution of the gas products obtained over all the catalysts. The products of methanol conversion reaction vary with the catalysts used. In general, the gas products mainly contain H_2, CO, CO_2, CH_4 and small portion of gaseous hydrocarbons such as C_2H_4, C_2H_6, C_3H_6, and C_3H_8. For both ZnO and Mn_3O_4, the main gas products are H_2 and CO, which are similar to the case without adding catalyst, however, the amounts of the obtained gas product over these two catalysts are obviously larger than that obtained in the blank experiment (Table 2), indicating that ZnO and Mn_3O_4 catalysts can promote the methanol reforming reaction (Eq.(2)).[31, 32] Meanwhile, the NiO and Co_3O_4 catalysts are observed to promote production of CH_4 and CO_2, suggesting the occurrence of both the water-gas shift (Eq.(3)) and the methanation reactions (Eq.(4), (5), (6)). Moreover, the product distribution over the Fe_3O_4 catalyst is similar to that obtained in the blank experiment, just with lower H_2 and CO but higher CH_4 and CO_2 yields. This indicates that adding Fe_3O_4 catalyst not only catalyze methanol reforming reaction but also facilitates the methanation reaction and water-gas shift reaction. The gas product compositions over $ZnFe_2O_4$ and $MnFe_2O_4$ catalysts are similar to that over Fe_3O_4 catalyst, and in contrast, the $NiFe_2O_4$ and $CoFe_2O_4$ catalysts promote the production of CH_4. Compared with that of the MFe_2O_4 catalysts (except $NiFe_2O_4$), the yields of H_2 and CO are decreased, but that of CH_4 is increased over the $M_{0.5}Co_{0.5}Fe_2O_4$ catalysts, indicating that adding the third metal element Co promotes the methanation reaction. Furthermore, a small amount of gaseous hydrocarbons such as C_2H_4, C_2H_6, C_3H_6, and C_3H_8 are formed over all

the catalysts. These hydrocarbons may stem from the pyrolysis of higher hydrocarbon or the Fischer-Tropsch synthesis.

Fig. 4b presents the liquid product distribution in the methanol conversion over all the catalysts. The main liquid products are a mixture of different compounds, such as C6–C21 hydrocarbons, alcohols, esters and ketones. There is nearly no liquid product in the absence of any catalyst (blank test in Fig. 4b). Likewise, the yields of liquid products over most of the MO catalysts are also very low except for the Co_3O_4 and Fe_3O_4 catalysts. Especially, Fe_3O_4 catalyst shows relatively high selectivity for C6–C21 hydrocarbons. Compared with that of Fe_3O_4, the yields of liquid products over $ZnFe_2O_4$, $MnFe_2O_4$ and $CoFe_2O_4$ catalysts are increased generally and the major liquid products are C6–C21 hydrocarbons (Table S2). In contrast, the yields of liquid products over $NiFe_2O_4$ catalyst are lower than that over Fe_3O_4, which may be because the addition of Ni promotes the methanation reaction and most of the syngas is converted to CH_4 (Fig. 4a). Additionally, compared to the MFe_2O_4 (M = Ni, Zn, Mn) catalysts, the addition of the third metal Co does not further increases the yields of the liquid products. In particular, $Ni_{0.5}Co_{0.5}Fe_2O_4$ shows a very low yield of C6–C21 hydrocarbons (Table S3 and Fig. 4b). This is because Ni and Co species can significantly promote syngas conversion to methanation, which is a competitive reaction to FTS. Among all these catalysts, $ZnFe_2O_4$ catalyst exhibits the highest yield of C6–C21 hydrocarbons. Based on the results of peak area (%) in Table S2-S3, the relative content of C6–C21 hydrocarbons over $ZnFe_2O_4$ is also the highest in the liquid products.

3.3. Reaction pathways analysis

The mechanism for methanol conversion to hydrocarbons over all the catalysts is complicated. As shown in Scheme 1, we propose the reaction pathways involved in the conversion of methanol over

all the catalyst based on the above catalytic results and product distributions. The formation of gas products from CH_3OH may involves the reaction of methanol reforming (Eq.(2))[31] to produce CO and H_2, and the water-gas shift reaction in which CO reacts with water to form CO_2 and H_2 (Eq.(3)),[33, 34] as well as the methanation reaction (Eq.(4), (5), (6)):[35]

$$CH_3OH \rightleftarrows 2H_2+CO \quad (2)$$

$$CO+H_2O \rightleftarrows CO_2+H_2 \quad (3)$$

$$CO+3H_2 \rightleftarrows CH_4+H_2O \quad (4)$$

$$2CO+2H_2 \rightleftarrows CH_4+CO_2 \quad (5)$$

$$CO_2+4H_2 \rightleftarrows CH_4+2H_2O \quad (6)$$

In methanol reforming reaction process, methanol is rapidly decomposed into CO and H_2. In this step, different catalysts result in different conversations and gas compositions. As we can see from Table 2 and Fig. 4, the MFe_2O_4 and $M_{0.5}Co_{0.5}Fe_2O_4$ catalysts generate higher conversations and more gas products as compared with Fe_3O_4 catalyst, and the Ni, Co and Fe containing catalysts are more favorable to producing CH_4. Additionally, the Fe-containing catalysts generate more CO_2 product as compared with the others. Therefore, we can conclude that the catalysts containing Zn, Ni, Mn, Co and Fe element can promote methanol reforming reaction,[24, 31, 32, 36-38] while the catalysts containing Ni, Co and Fe element can promote the subsequent methanation reaction,[39-41] and the Fe-containing catalysts promote water-gas shift reaction.[42] Subsequently, the hydrogen in the gas products of methanol reforming can be converted to hydrocarbons via Fischer–Tropsch synthesis (FTS). The main reactions during FTS can be expressed in Equations (7), (8), (9) and (10):

$$(2n+1)H_2+nCO \rightarrow C_nH_{2n+2}+nH_2O \quad (7)$$

$$2nH_2+nCO \rightarrow C_nH_{2n}+nH_2O \quad (8)$$

$$nCO+2nH_2 \rightarrow CnH_{2n+1}OH+(n-1)H_2O \quad (9)$$

$$(n+1)CO+(2n+1)H_2 \rightarrow C_nH_{2n+1}CHO+nH_2O \quad (10)$$

In the FTS process, firstly, CO and H_2 are converted to intermediate-1 through hydrogenation and dehydration reaction. Subsequently, the intermediate-1 is further converted via a series of successive or parallel steps. On the one hand, the intermediate-1 can be converted to intermediate-2 through hydrogenation and dehydration reaction,[18] and then the intermediate-2 is further converted to alkanes and olefins by hydrogenation or dehydrogenation. In the process of CO and H_2 conversion to hydrocarbons, only Co_3O_4 and Fe_3O_4 among the MO catalysts show the high catalytic activity with a high selectivity towards C6–C21 hydrocarbons. The reason may be that Co_3O_4 and Fe_3O_4 catalyst accelerate the hydrogenation and dehydrogenation of intermediate-1 to hydrocarbons. Moreover, the addition of $ZnFe_2O_4$, $MnFe_2O_4$ and $CoFe_2O_4$ catalysts not only promoted the hydrogenation,[43-45] but also promoted dehydration reaction,[46-48] both of which are favorable for the production of hydrocarbons, and thus adding these three catalysts can increase the yield of hydrocarbons. However, the $Mn_{0.5}Co_{0.5}Fe_2O_4$ and $Zn_{0.5}Co_{0.5}Fe_2O_4$ catalysts can decrease the yield of hydrocarbons as compared with the MFe_2O_4 catalyst. This is because Co species can significantly promote syngas conversion to methanation, which is a competitive reaction to FTS. On the other hand, the intermediate-1 also can be converted to oxygenated compounds directly, such as aldehydes, alcohols, which can be explained by the CO insertion mechanism. Additionally, the ketones can be formed through two ways. One is that alcohols react with intermediate1 to form ketones (see red solid line of Scheme 1), and the other is that aldehydes are converted to carboxylic acid via cannizzaro reaction, and then the formed carboxylic acid reacts with alcohols to form ketones (see green solid lines of Scheme 1).[49] As we investigated, ZnO showed a significant activity in hydrogenation of ethylene, and also was effective to catalyze the dehydration of glycerol to yield

acetol.[43, 46] Likewise, in our reaction system, $ZnFe_2O_4$ is identified as the most effective catalyst for conversion of methanol to C6–C21 hydrocarbons, due to its catalytic capability for the hydrogenation and dehydration reactions. Therefore, it can conclude that catalyst compositions greatly affect the yield and distribution of both gas and liquid products. $ZnFe_2O_4$ exhibits the best catalytic activity among all the examined catalysts. The following study was therefore focusing on the conversion of methanol over $ZnFe_2O_4$.

3.4. Methanol conversion over $ZnFe_2O_4$ catalyst

3.4.1. Effect of reaction temperature

Table 3 (entries 1-6) shows the effect of the reaction temperature on the conversion of methanol and the gas products. When the reaction temperature is 220 ^oC (not shown here), negligible amount of the gas products is collected, indicating that the methanol reforming reaction is still not initiated at this temperature. With increase of the reaction temperature from 240 to 340 ^oC, both the methanol conversion and the gas products are increased gradually, and then maintained at a certain value. These results suggest higher reaction temperature favors the production of gas products in the temperature range from 220 to 320 ^oC.

Fig. 5a shows the influence of the reaction temperature on the gas product distribution in methanol conversion over the $ZnFe_2O_4$ catalyst. Around 240 ^oC, H_2 and CO are detected as the main products, because the methanol reforming reaction is likely to occur at this temperature. Further increasing the reaction temperature leads to the decrease of CO and H_2 yield but also simultaneously to the rising up both the CO_2 and CH_4 yield, because of the occurrence of methanation reaction and water-gas shift reaction which convert CO and H_2 to CO_2 and CH_4. The yield of CO_2 and CH_4 is highly dependent on the increase of the reaction temperature, indicating a

relative higher temperature is in favor of the water-gas shift and methanation reaction in the examined temperature window. When the temperature is above 300 ^{o}C, the yield of CO_2 is almost not changed, while that of H_2 is decreased gradually, and those of ethane and propane are increased more obviously due to FTS. Fig. 5b shows the distribution of liquid products at different reaction temperatures. It reveals that the yield of C6–C21 hydrocarbons is increased with the change of the reaction temperature from 240 to 300 ^{o}C, but the increment becomes very small at higher reaction temperatures. Additionally, when the temperature is above 300 ^{o}C, more ketone is formed. This can be attributed to the occurrence of the competitive reactions, which are promoted at high temperature leading to the formation of byproducts and more gas products.[50] Based on the measured peak areas (%) in Table S4, the main liquid products over $ZnFe_2O_4$ catalyst are C6–C21 hydrocarbons at 240-340 ^{o}C, including straight chain hydrocarbon and their derivatives. The relative content of C6–C21 hydrocarbons is as high as 100 % when the reaction temperature is below 260 ^{o}C. It is noteworthy that with the increase of the reaction temperature, the relative content of low carbon number hydrocarbons become higher, and simultaneously, the relative content of C14-C21 hydrocarbons becomes lower (entries 37-45 in Table S4), suggesting that the high carbon number hydrocarbons are decomposed to the ones with lower carbon numbers at higher reaction temperatures.[51] By comprehensively considering both the conversion of methanol and the yield of C6–C21 hydrocarbons, the optimum reaction temperature is determined to be ca. 300 ^{o}C.

3.4.2. Effect of reaction time

As shown in Table 3, the conversion of methanol reaches 19.2 % when the reaction time is 10 minutes (entry 7 in Table 3), suggesting that the reforming reaction of methanol to CO and H_2 did occur under this reaction condition. As the reaction time is extended from 10 to 120 min, the

methanol conversion and the total amount of gas products (entries 4, 7–11 in Table 3) are increased gradually. However, these values are only slightly increased when the reaction time is further extended to 240 min. Fig. 6a shows that the distribution of gas products is obviously changed with reaction time, indicating that reaction time has much effect on gas product distribution. With the reaction time increasing from 10 to 240 min, the relative amounts of H_2 and CO in gas products become lower, while those of CH_4 and CO_2 become higher. This may be because the active sites of methanation are formed simultaneously with the reaction under the reaction conditions.[52] The effect of reaction time on the distribution of liquid products is presented in Fig. 6b. The effect of reaction time on the distribution of liquid products is presented in Fig. 6b. It can be seen that the yields of both the total liquid products and the C6–C21 hydrocarbons become higher with the reaction time increasing from 10 to 120min, indicating in the initial stage of the reaction, the FT synthetic is the dominant reaction. When the reaction time is longer than 120 min, there is little change for the peak area values of C6–C21 hydrocarbons, suggesting that it has reached equilibrium between the FT synthetic and decomposition reactions of hydrocarbons. Table S5 demonstrates that as the reaction time is above 180 min, the relative content of low carbon number hydrocarbons becomes higher, while that of C14-C21 hydrocarbons becomes lower (entries 33-43 in Table S5), confirming that these hydrocarbons are decomposed into hydrocarbons with lower carbon numbers at longer reaction time. Accordingly, based on the conversion of methanol and the yield of C6–C21 hydrocarbons, the optimized reaction time is 120 min.

3.4.3. Effect of catalyst amount

As shown in Table 3 (entries 10, 12–14), both the conversion of methanol and total amount of the gas product are increased with the addition of more catalyst but not in a proportional way. Fig. 7a

shows the effect of catalyst amount on the distribution of gas products. It reveals that the volume fraction of CH_4 is increased but that of H_2 and CO decreased drastically with the addition of more catalyst, which is attributed to the fact that with addition of more catalyst, it will provide more active sites for methanation reaction, which will consume more H_2 and CO. Fig. 7b presents the distribution of the liquid products against the catalyst amount. When the catalyst amount is changed from 0.1 to 0.5 g, there is a gradual increase in the yield of C6–C21 hydrocarbons. With further addition of the catalyst, the yield of C6–C21 hydrocarbons becomes a little higher and more by-products such as ketones and alcohols are formed. As shown in Table S6, the relative content of C6–C21 hydrocarbons keeps at about 97% when the catalyst content is maintained below 0.5 g; however, it declines to 91% as the catalyst amount is increased to 0.9 g. The reason should be that although the increased amount of catalyst can provide more active sites for the methanol reforming and subsequent FTS reactions, the excess catalyst further promotes decomposition of hydrocarbons to by-products and gas products.[53] Considering both the conversion of methanol and the yield of C6–C21 hydrocarbons, the optimized catalyst amount is 0.5 g.

3.4.4. Catalytic stability of the $ZnFe_2O_4$ catalyst

Fig. 8 shows the catalytic activity of $ZnFe_2O_4$ catalyst for the methanol conversion undergoing four runs. It reveals that the distribution of gas products changes somewhat in these four circles, while that of the liquid products is not changed obviously in the next three circles. In the next three stability tests, a little amount of catalyst is inevitably lost. The distribution of C6–C21 hydrocarbons in liquid products is also similar in the four circles (Table S7). These results indicate that $ZnFe_2O_4$ catalyst is relatively stable and reusable under the reaction condition used in this work.

4. Conclusions

In summary, it has demonstrated that methanol can be efficiently converted to C6–C21 hydrocarbons over the bi-functional Fe-based spinel catalysts synthesized by a facile solvothermal method, in which the Fe-based spinel catalysts play dual roles: (i) catalyzing methanol reforming to generate H_2 and CO, and then (ii) converting these gas products to hydrocarbons through Fischer-Tropsch reaction. The $MnFe_2O_4$, $ZnFe_2O_4$ catalysts enhance the production of C6–C21 hydrocarbons while $NiFe_2O_4$ and $CoFe_2O_4$ catalysts promote the formation of more gas products such as CH_4 and CO_2. It is found that all the used MO catalysts promote methanol reforming reaction except that Co_3O_4 and Fe_3O_4 favor for FTS. Comparing with the Fe-based spinel catalysts, further doping of Co to the spinel structure does not improve the catalytic activity. On the contrary, $Ni_{0.5}Co_{0.5}Fe_2O_4$ has lower catalytic activity as compared with the Fe_3O_4 catalyst, because Co species can significantly promote syngas conversion to methanation, which is a competitive reaction to FTS. Among these catalysts, $ZnFe_2O_4$ catalyst exhibits the highest catalytic activity and yield towards C6–C21 hydrocarbons. The stability test shows that the $ZnFe_2O_4$ catalyst is stable and reusable under the reaction conditions. This work provides a new promising route to convert abundant renewable methanol to liquid fuels by one-pot reaction. Further work in selection of supports for the $ZnFe_2O_4$ active component for further increasing the yield and selectivity towards the liquid products is undergoing.

Acknowledgements

This work was supported by the Major State Basic Research Development Program of China (973 Project) (Nos. 2011CB200906 and 2014CB744306), National Natural Science Foundation of China (No. 21161140329), National High Technology Research and Development Program of

China (863) (No. SS2012AA021402), and "Strategic Priority Research Program" of the Chinese Academy of Sciences (Nos. XDA07010100 and XDA07010200).

References

1 C. N. Hamelinck and A. P. Faaij, *J. Power Sources*, 2002, **111**, 1–22.

2 Z. X. Wang, T. Dong, L. X. Yuan, T. Kan, X. F. Zhu, Y. Torimoto, M. Sadakata and Q. X. Li, *Energy Fuels*, 2007, **21**, 2421–2432.

3 H. Kobayashi, N. Takezawa and C. Minochi, *J. Catal.*, 1981, **69**, 487–494.

4 H. Agaras, G. Cerrella and M. Laborde, *Appl. Catal.*, 1988, **45**, 53–60.

5 C. Fukuhara, Y. Kamata and A. Igarashi, *Appl. Catal.*, *A*, 2007, **330**, 108–116.

6 N. Iwasa, T. Mayanagi, N. Ogawa, K. Sakata and N. Takezawa, *Catal. Lett.*, 1998, **54**, 119–123.

7 A. M. Karim, T. Conant and A. K. Datye, *Phys. Chem. Chem. Phys.*, 2008, **10**, 5584–5590.

8 C. Z. Yao, L. C. Wang, Y. M. Liu, G. S. Wu, Y. Cao, W. L. Dai, H. Y. He and K. N. Fan, *Appl. Catal.*, *A*, 2006, **297**, 151–158.

9 D. R. Palo, R. A. Dagle and J. D. Holladay, *Chem. Rev.*, 2007, **107**, 3992–4021.

10 S. Sá, H. Silva, L. Brandão, J. M. Sousa and A. Mendes, *Appl. Catal.*, *B*, 2010, **99**, 43–57.

11 A. Y. Khodakov, W. Chu and P. Fongarland, *Chem. Rev.*, 2007, **107**, 1692–1744.

12 J. M. Gonzalez Carballo, E. Finocchio, S. Garcia-Rodriguez, M. Ojeda, J. L. Garcia Fierro and S. Rojas, *Catal. Today*, 2013, **214**, 2–11.

13 E. Iglesia, S. L. Soled and R. A. Fiato, *J. Catal.*, 1992, **137**, 212–224.

14 R. A. Dictor and A. T. Bell, *J. Catal.*, 1986, **97**, 121–136.

15 C. K. Rofer-DePoorter, *Chem. Rev.*, 1981, **81**, 447–474.

16 S. Li, S. Krishnamoorthy, A. Li, G. D. Meitzner and E. Iglesia, *J. Catal.*, 2002, **206**, 202–217.

17 E. Iglesia, S. L. Soled, R. A. Fiato and G. H. Via, *J. Catal.*, 1993, **143**, 345–368.

18 H. Schulz, *Appl. Catal.*, *A*, 1999, **186**, 3–12.

19 M. E. Dry, *Appl. Catal.*, *A*, 2004, **276**, 1–3.

20 B. Jager, P. Van Berge and A. P. Steynberg, in *Stud. Surf. Sci. Catal.*, 2001, **136**, 63–68.

21 Z. L. Zhang, Q. Q. Tan, Y. F. Chen, J. Yang and F. B. Su, *J. Mater. Chem.*, *A*, 2014, **2**, 5041–5050.

22 C.Q. Dong, Z.F. Zhang, Q. Lu and Y.P. Yang, *Energy Convers. Manage.*, 2012, **57**, 49–59.

23 A. Pattiya, J. O. Titiloye and A. V. Bridgwater, *J. Anal. Appl. Pyrolysis*, 2008, **81**, 72–79.

24 Y. H. Wu, F. N. Gu, G. W. Xu, Z. Y. Zhong and F. B. Su, *Bioresour. Technol.*, 2013, **137**, 311–317.

25 K. Maaz, S. Karim, K. J. Lee, M. H. Jung and G. H. Kim, *Mater. Chem. Phys.*, 2012, **133**, 1006–1010.

26 K. Verma, A. Kumar and D. Varshney, *J. Alloys Compd.*, 2012, **526**, 91–97.

27 H. M. I. Abdallah, T. Moyo and J. Z. Msomi, *J. Phys. Conf. Ser.*, 2010, **217**, 012141.

28 B. H. Davis, *Catal. Today*, 2009, **141**, 25–33.

29 S. Bera, A. A. M. Prince, S. Velmurugan, P. S. Raghavan, R. Gopalan G. Panerslvam and S. V,.Narasihan, *J. Mater. Sci.*, 2001, **36**, 5379– 384.

30 Z. Xing, Z. C. Ju, J. Yang, H. Y. Xu and Y.T. Qian, *Nano. Res.*, 2012, **5**, 477–485.

31 D. V. César, R. F. Robertson and N. S. Resende, *Catal. Today*, 2008, **133-135**, 136–141.

32 R. O. Idem and N. N. Bakhshi, *Chem. Eng. Sci.*, 1996, **51**, 3697–3708.

33 J. Amelse, L. Schwartz and J. Butt, *J. Catal.*, 1981, **72**, 95–110.

34 G. Chinchen, R. Logan and M. Spencer, *Appl. Catal.*, 1984, **12**, 89–96.

35 M. Araki and V. Ponec, *J. Catal.*, 1976, **44**, 439–448.

36 M. Mrad, D. Hammoud, C. Gennequin, A. Aboukais and E. Abi-Aad, *Appl. Catal.*, *A*, 2014, **471**, 84–90.

37 N. Laosiripojana and S. Assabumrungrat, *J. Power Sources*, 2007, **163**, 943–951.

38 E. Manova, T. Tsoncheva, C. Estournès, D. Paneva, K. Tenchev, I. Mitov and L. Petrov, *Appl. Catal., A*, 2006, **300**, 170–180.

39 R. Hayes, W. Thomas and K. Hayes, *J. Catal.*, 1985, **92**, 312–326.

40 P. K. Agrawal, J. R. Katzer and W. H. Manogue, *J. Catal.*, 1981, **69**, 312–326.

41 A. L. Kustov, A. M. Frey, K. E. Larsen, T. Johannessen, J. K. Norskov and C. H. Christensen, *Appl. Catal.*, *A*, 2007, **320**, 98–104.

42 D. S. Newsome, *Catal. Rev. Sci. Eng.*, 1980, **21**, 275–318.

43. A. Dent and R. Kokes, *J Phys. Chem.*, 1969, **73**, 3781–3790.

44 H. Itoh, S. Nagano, K. Takeda and E. Kikuchi, *Appl. Catal.*, *A*, 1993, **96**, 125–134.

45 D. Schanke, S. Vada, E. Blekkan, A. Hilmen, A. Hoff and A. Holmen, *J. Catal.*, 1995, **156**, 85–95.

46 M. Balaraju, V. Rekha, P. S. Prasad, R. Prasad and N. Lingaiah, *Catal. Lett.*, 2008, **126**, 119–124.

47 S. Hocevar, J. Batista and V. Kaucic, *J. Catal.*, 1993, **139**, 351–361.

48 P. J. Skrdla and R. T. Robertson, *J. Mol. Catal. A: Chem.*, 2003, **194**, 255–265.

49 E. de Smit and B. M. Weckhuysen, *Chem. Soc. Rev.*, 2008, **37**, 2758–2781.

50 A. A. Mirzaei, B. Shirzadi, H. Atashi and M. Mansouri, *J. Ind. Eng. Chem.*, 2012, **18**, 1515–1521.

51 J. S. Kim, S. Lee, S. B. Lee, M. J. Choi and K. W. Lee, *Catal. Today*, 2006, **115**, 228–234.

52 C. W. Hu, J. Yao, H. Q. Yang, Y. Chen and A. M. Tian, *J. Catal.*, 1997, **166**, 1–7.

53 M. A. Dasari, P. P. Kiatsimkul, W. R. Sutterlin and G. J. Suppes, *Appl. Catal.*, *A*, 2005, **281**, 225–231

Figure Captions

Fig. 1 XRD patterns of all the catalysts (a-c), and H_2-TPR curves of $ZnFe_2O_4$, $MnFe_2O_4$, and $CoFe_2O_4$ catalysts (d).

Fig. 2 SEM images of the catalysts: (a) Fe_3O_4, (b) $NiFe_2O_4$, (c) $ZnFe_2O_4$, (d) $MnFe_2O_4$, (e) $CoFe_2O_4$, (f) $Ni_{0.5}Co_{0.5}Fe_2O_4$, (g) $Zn_{0.5}Co_{0.5}Fe_2O_4$, and (h) $Mn_{0.5}Co_{0.5}Fe_2O_4$.

Fig. 3 TEM image of $ZnFe_2O_4$ (a), HRTEM image of $ZnFe_2O_4$ (b), SEM image and elemental mapping images of O, Zn and Fe for $ZnFe_2O_4$ nanoparticles (c), and SEM-EDX spectrum (d).

Fig. 4 Distribution of gas (a) and liquid (b) products over all the catalysts. (Reaction conditions: 0.5 g catalyst, 30 mL methanol, 180 min, 280 ^oC.)

Fig. 5 Effect of reaction temperature on the distribution of gas (a) and liquid (b) products over $ZnFe_2O_4$ catalyst. (Reaction conditions: 0.5 g catalyst, 30 mL methanol, 180 min, 240-340 ^oC.)

Fig. 6 Effect of reaction time on the distribution of gas (a) and liquid (b) products over $ZnFe_2O_4$ catalyst. (Reaction conditions: 0.5 g catalyst, 30 mL methanol, 300 ^oC, 1–240 min.)

Fig. 7 Effect of catalyst amount on the distribution of gas (a) and liquid (b) products over $ZnFe_2O_4$ catalyst. (Reaction conditions: 0.1–0.9 g catalyst, 30 mL methanol, 120 min, 300 ^oC.)

Fig. 8 Distribution of gas (a) and liquid (b) products over 4 circles over $ZnFe_2O_4$ catalyst. (Reaction conditions: 0.5 g catalyst, 30 mL methanol, 120 min, 300 ^oC.)

Scheme 1 Proposed reaction pathways for conversion of methanol over iron-based catalysts.

Table 1 Physicochemical properties of all the catalysts.

Sample	S_{BET} [a] (m^2 g^{-1})	Crystal size [b] (nm)
NiO	4.5	42.9
ZnO	0.5	102.1
Mn_3O_4	45.2	41.9
Co_3O_4	0.1	82.8
Fe_3O_4	5.7	92.8
$NiFe_2O_4$	76.5	11.6
$ZnFe_2O_4$	21.1	29.4
$MnFe_2O_4$	40.1	19.2
$CoFe_2O_4$	63.1	11.9
$Ni_{0.5}Co_{0.5}Fe_2O_4$	69.8	14.7
$Zn_{0.5}Co_{0.5}Fe_2O_4$	66.3	18.4
$Mn_{0.5}Co_{0.5}Fe_2O_4$	49.2	21.6

[a] Surface area, derived from BET equation. [b] Crystal size, derived from XRD by Debye−Scherrer equation.

Table 2 Conversion of methanol and the total gas product mass over MO, MFe_2O_4 and $M_{0.5}Co_{0.5}Fe_2O_4$ catalysts.

Catalyst	Conversion (%)[a]	Total gas mass (g)
Without catalyst	8.9	1.8
NiO	26.6	6.1
ZnO	12.0	2.9
Mn_3O_4	11.3	2.8
Co_3O_4	35.9	6.1
Fe_3O_4	19.4	4.7
$NiFe_2O_4$	29.7	6.5
$ZnFe_2O_4$	26.2	5.6
$MnFe_2O_4$	22.1	4.8
$CoFe_2O_4$	24.2	4.2
$Ni_{0.5}Co_{0.5}Fe_2O_4$	24.8	4.6
$Zn_{0.5}Co_{0.5}Fe_2O_4$	22.8	4.0
$Mn_{0.5}Co_{0.5}Fe_2O_4$	27.3	4.8

[a] Reaction conditions: 0.5 g catalyst, 30 mL methanol, 180 min, 280 ^oC.

Table 3 Effect of reaction conditions on the conversion of methanol over $ZnFe_2O_4$ catalyst.

Entry	Reaction temperature (^oC)	Reaction Time (min)	Catalyst amount (g)	Conversion (%)	Total gas mass (g)
1	240	180	0.5	17.0	4.1
2	260	180	0.5	22.5	5.1
3	280	180	0.5	26.2	5.6
4	300	180	0.5	26.7	5.7
5	320	180	0.5	27.9	5.8
6	340	180	0.5	27.8	5.8
7	300	10	0.5	19.2	4.7
8	300	30	0.5	21.8	5.0
9	300	60	0.5	23.8	5.3
10	300	120	0.5	26.1	5.6
11	300	240	0.5	27.4	5.6
12	300	120	0.1	19.0	5.0
13	300	120	0.3	23.7	5.4
14	300	120	0.9	27.7	5.9
15	300	120	0.5	25.7	5.6
16	300	120	0.5	26.0	5.5
17	300	120	0.5	25.3	5.5

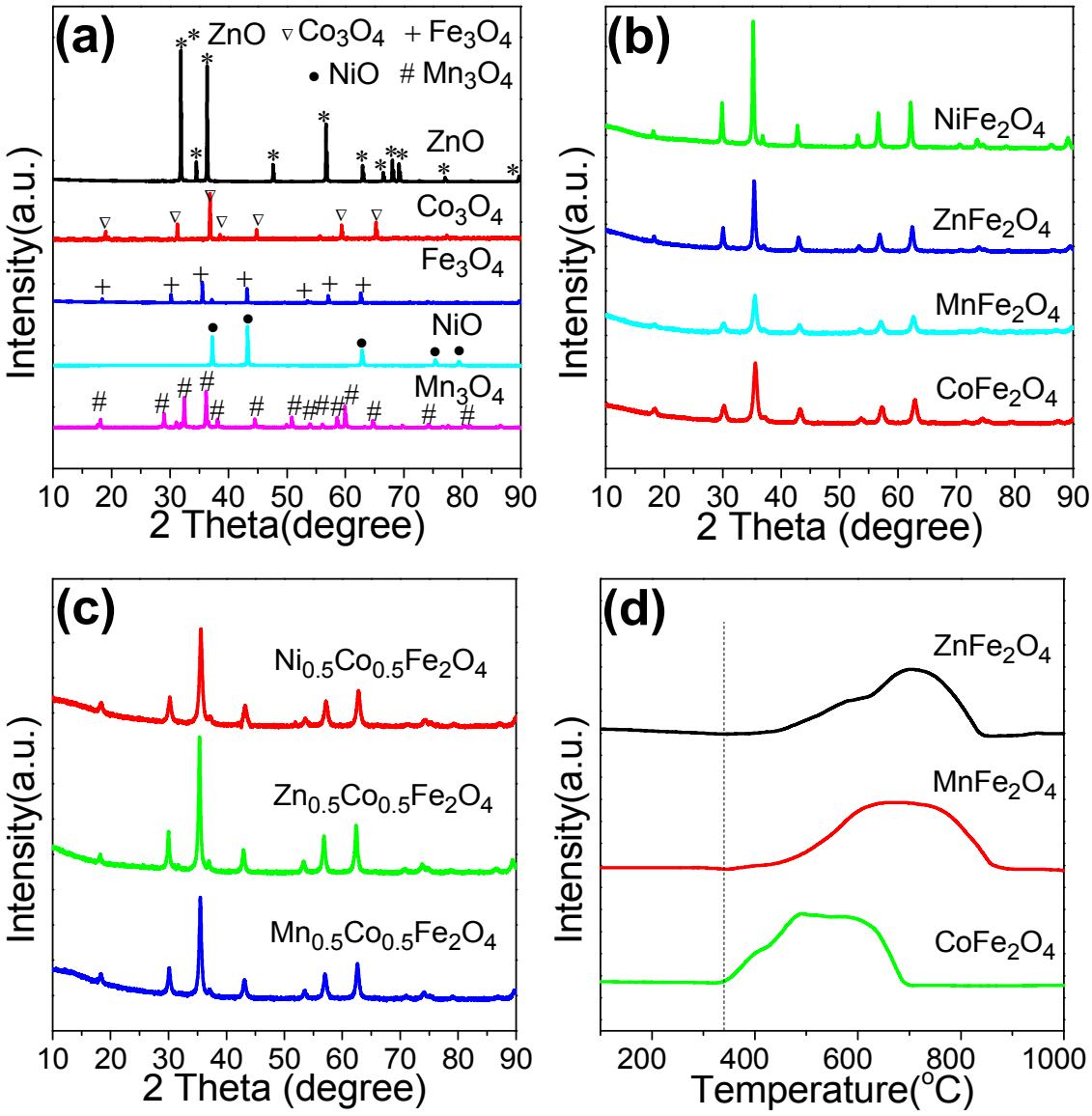

Fig. 1

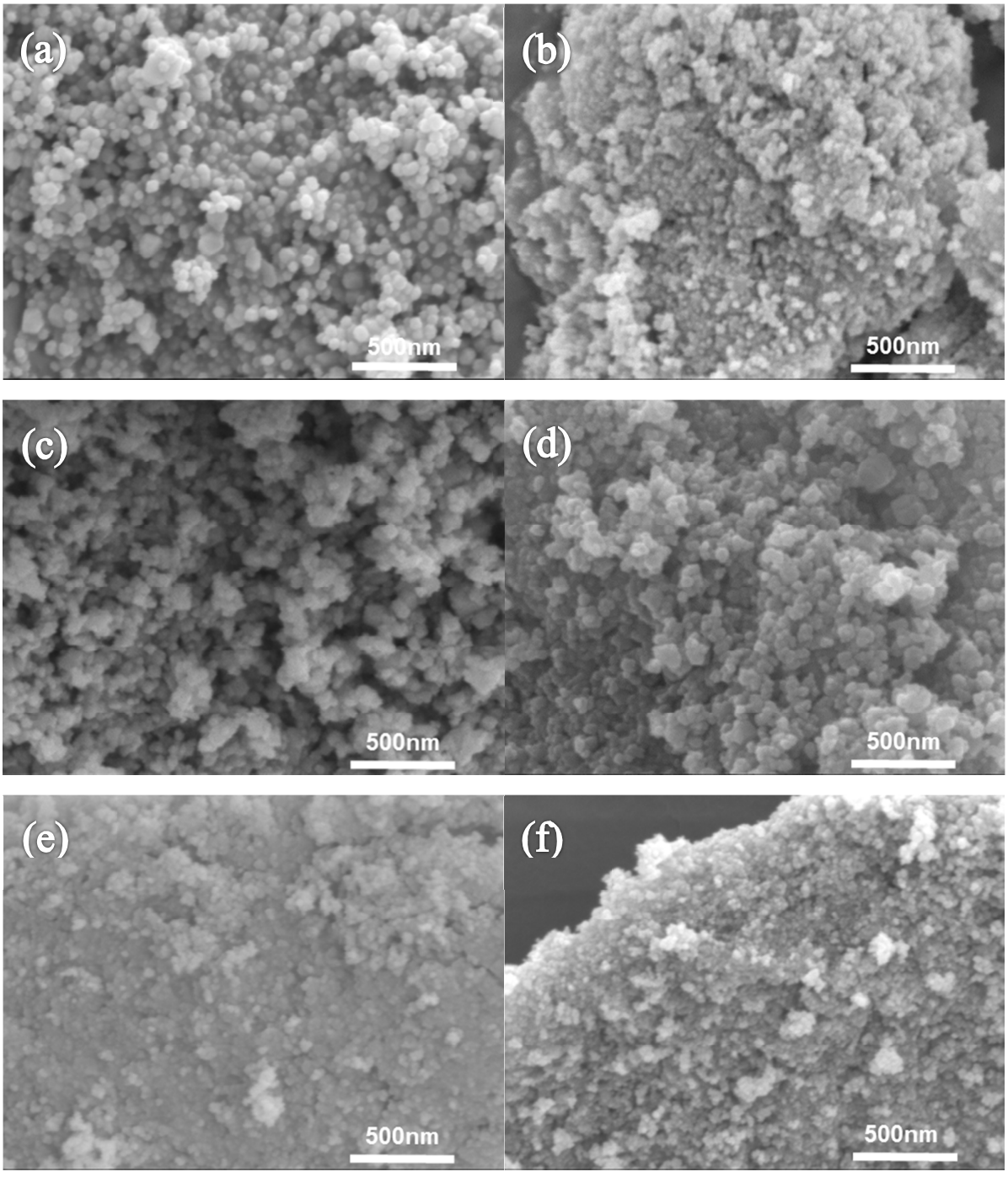

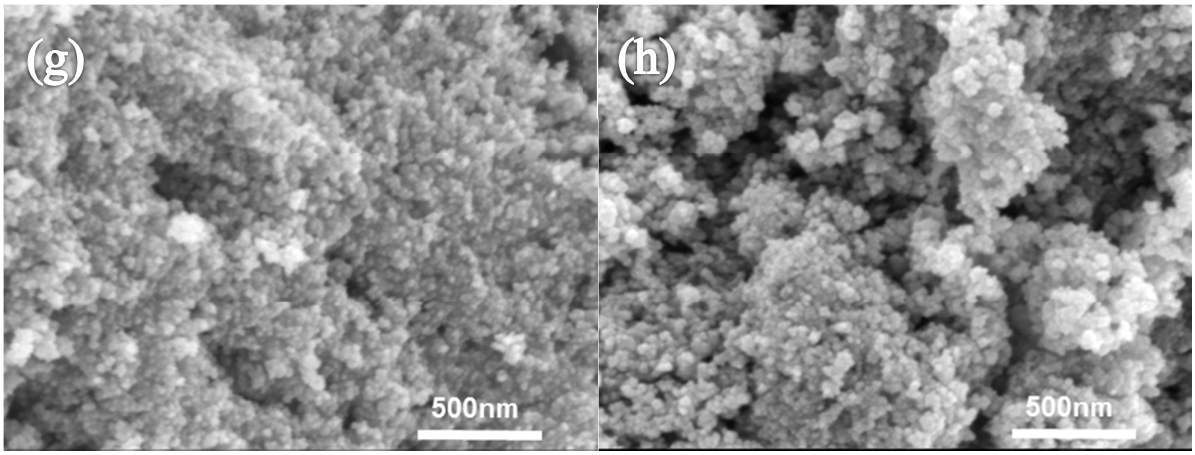

Fig. 2

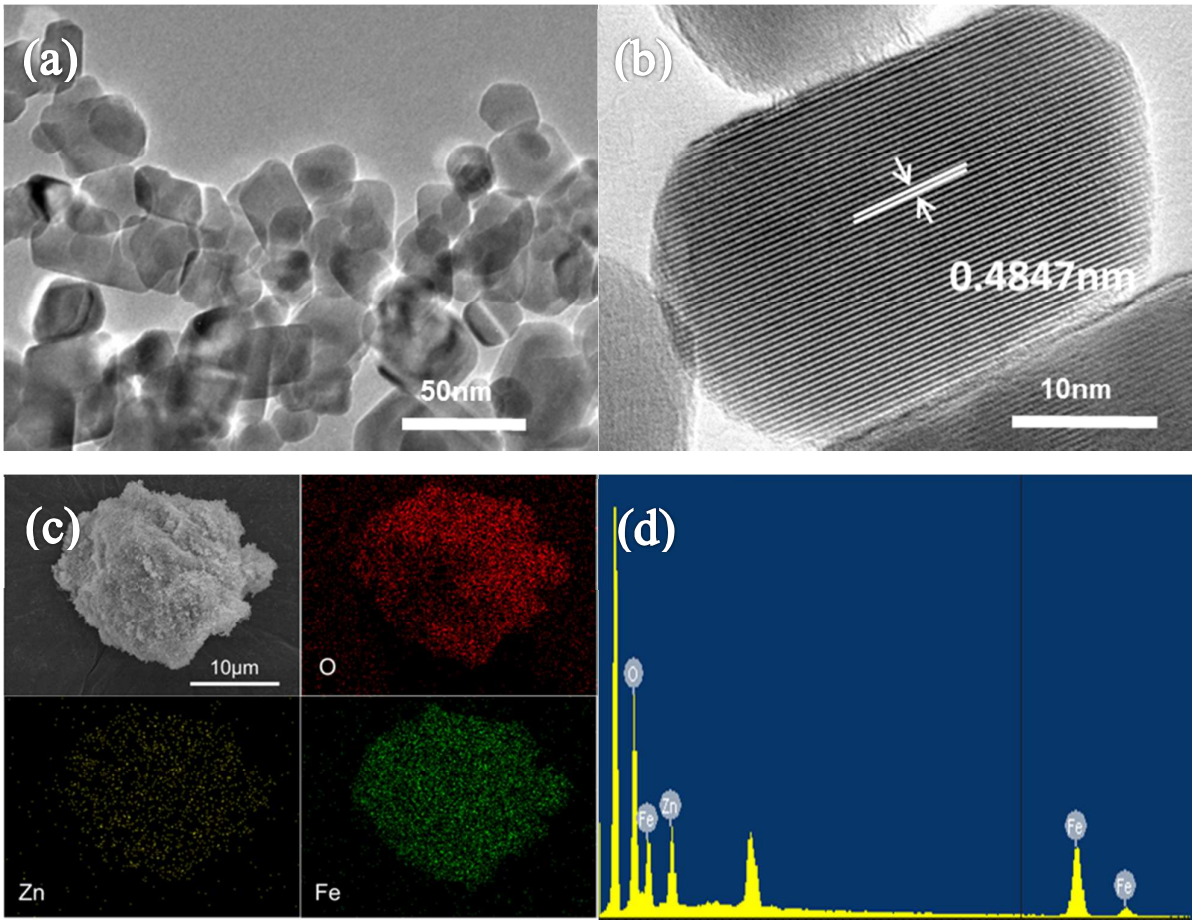

Fig. 3

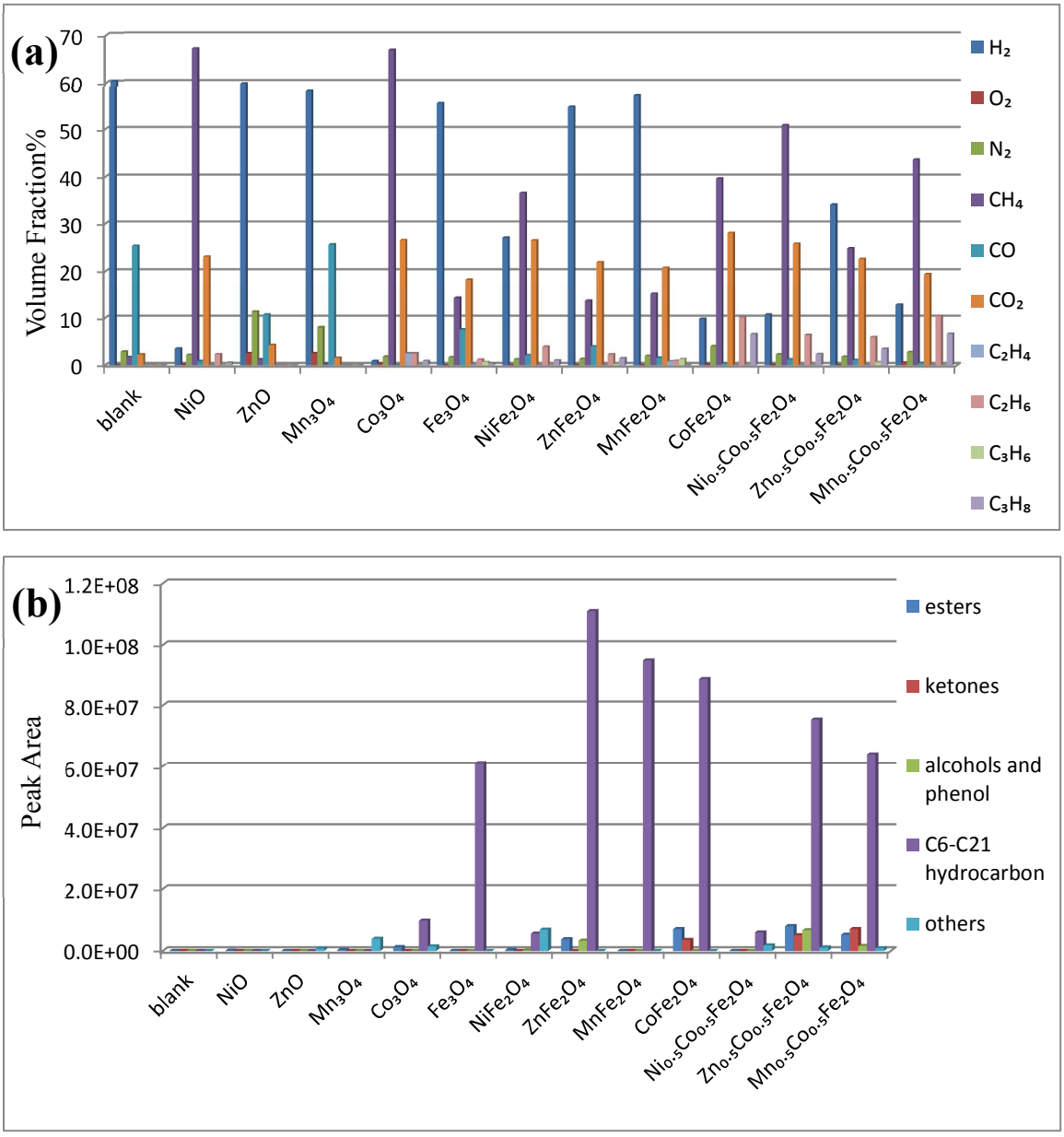

Fig. 4

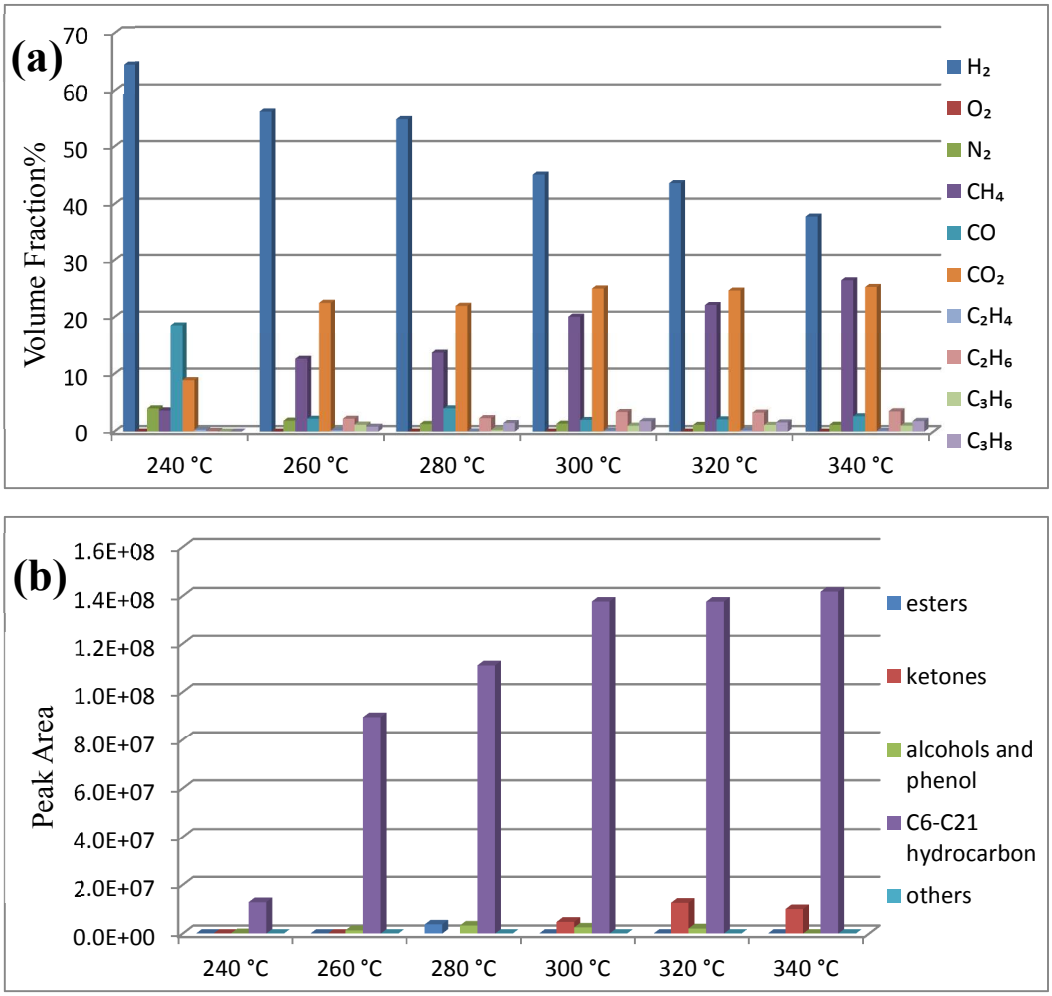

Fig. 5

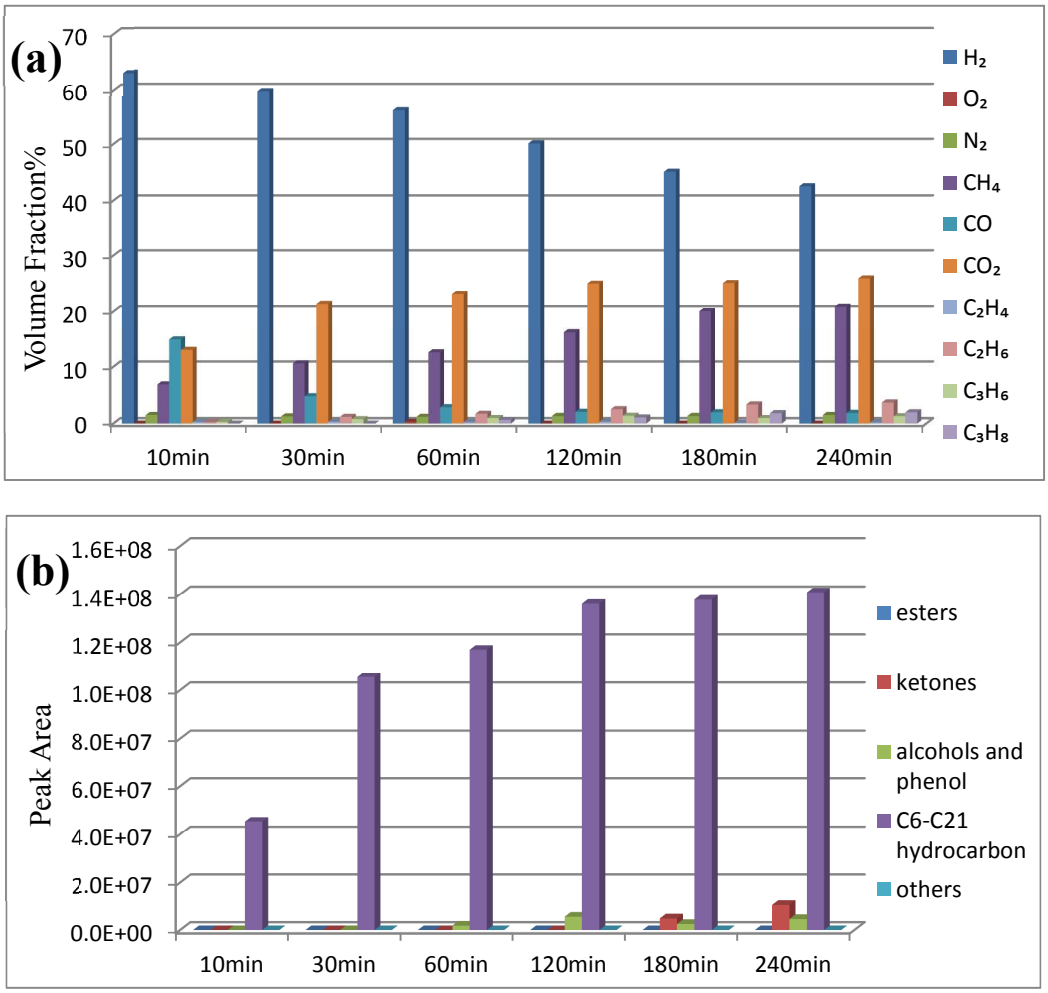

Fig. 6

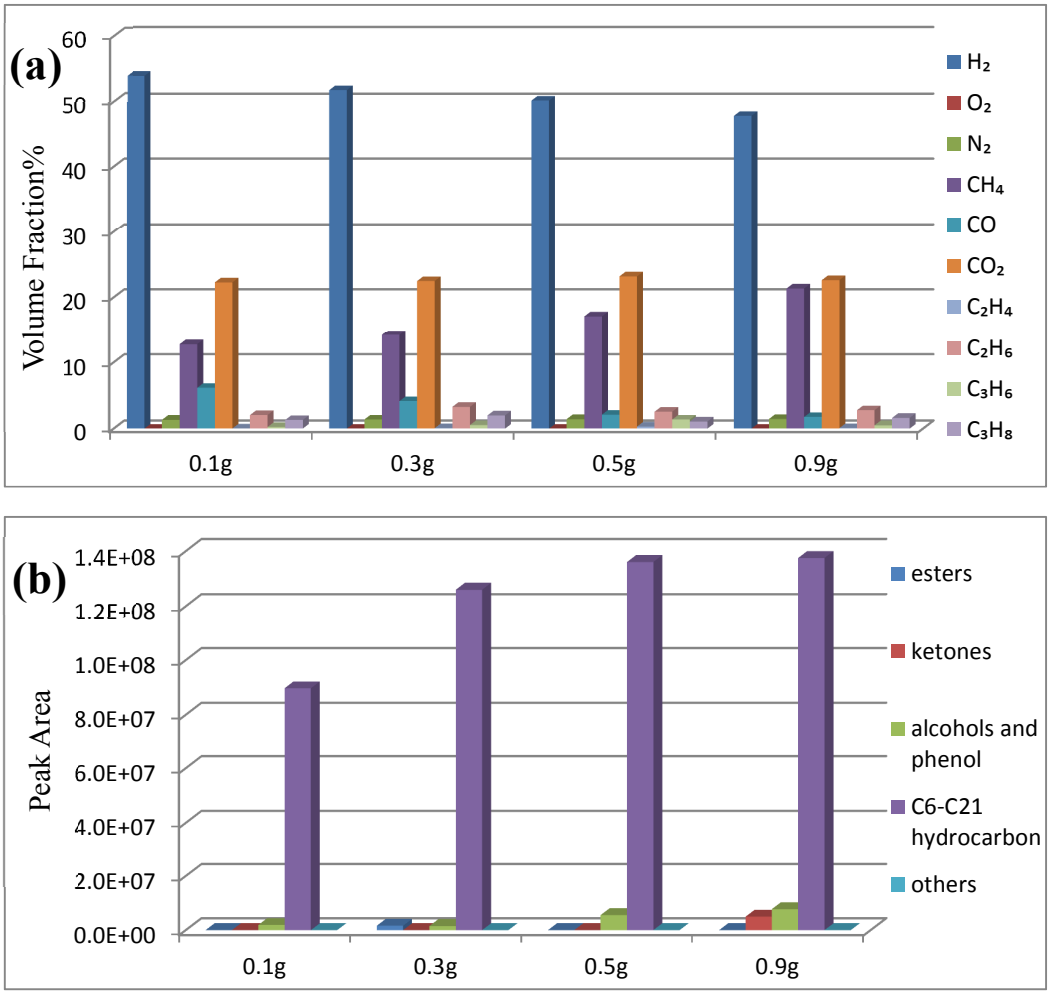

Fig. 7

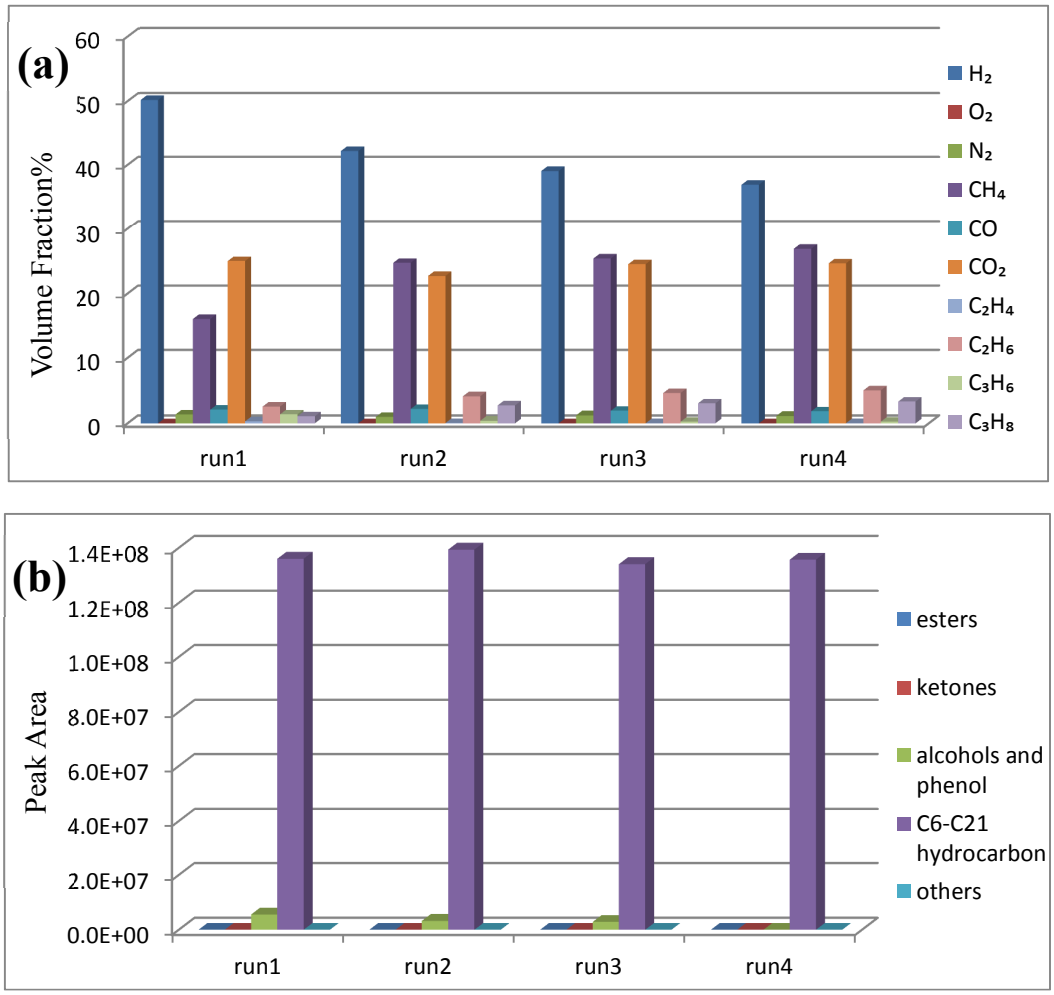

Fig. 8

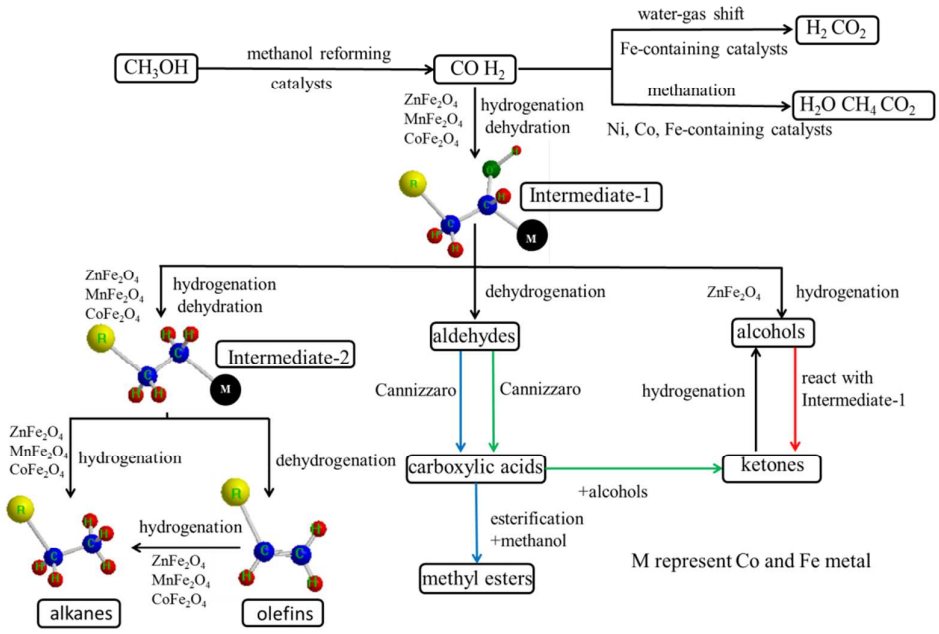

Scheme 1 Proposed reaction pathways for conversion of methanol over iron-based catalysts.